Desalination and Water Treatment
www.deswater.com
doi: 10.1080/19443994.2015.1094678

57 (2016) 18825–18835
August

Taylor & Francis
Taylor & Francis Group

The influence of carbonization temperature on the modification of TiO_2 in the removal of methyl orange from aqueous solution by adsorption

Shila Jafari[a,*], Bahareh Yahyaei[b], Ewelina Kusiak-Nejman[c], Mika Sillanpää[a]

[a]*Laboratory of Green Chemistry, LUT Chemistry, Lappeenranta University of Technology, Sammonkatu 12, FI-50130 Mikkeli, Finland, Tel. +358 504 332 348; email: Shila.jafari@lut.fi, shila.sanaz.jafari@gmail.com (S. Jafari), mika.sillanpää@lut.fi (M. Sillanpää)*
[b]*Faculty of Chemistry, Department of Physical Chemistry, Bu-Ali Sina University, Hamedan, Iran, email: bahareh.yahyaei@gmail.com*
[c]*Szczecin Institute of Inorganic Technology and Environment Engineering, West Pomeranian University of Technology, Szczecin, Poland, email: ewelina.Kusiak@zut.edu.pl*

Received 13 July 2015; Accepted 11 September 2015

ABSTRACT

This work investigated the adsorption ability of unmodified and carbon-modified TiO_2 nanoparticles for the removal of methyl orange (MO) from aqueous solution. Carbon–TiO_2 was obtained by carbonization of ethanol vapors at three different temperatures (200, 300, and 400°C), and their adsorption was compared with unmodified TiO_2 nanoparticles. The Freundlich adsorption model was found to fit for TiO_2 and C–TiO_2-200, while carbon modification of TiO_2 at a high temperature fitted the Langmuir–Freundlich model (C–TiO_2-300 and C–TiO_2-400). Generally, the carbonization of C–TiO_2 increased the adsorption capacity of TiO_2 nanoparticles, however the BET surface of modified and pristine TiO_2 was almost the same. The zeta potential of modified TiO_2 is higher than unmodified TiO_2, which leads to efficient adsorption of MO onto modified TiO_2.

Keywords: Methyl orange; Dye; TiO_2; Carbon modification; Zeta potential; Adsorption

1. Introduction

Environmental protection is the practice of protecting the natural environment, which is also of benefit to humans. Azo dyes are among the thousands of industrial dyes that break down to toxic products harmful to ecosystems and human health [1]. Thus, the efficient removal of these dye pollutants from wastewaters is very important.

Many types of biological and chemical process including ozonation [2], flocculation [3], coagulation [3,4], and adsorption [5–7] have been used to remove dye pollutants. Adsorption is simple, low cost, and in many cases the most effective of these.

Although activated carbon is one of the most efficient adsorbents for different types of pollutant, it is expensive, usually time-consuming, and complicated to prepare. Thus, many attempts have been made to find economical yet effective adsorbents. Nano-adsorbents are highly efficient and have been extensively used for dye removal. The very high surface area to volume ratio of many nanomaterials makes them extremely advantageous as adsorbents. For example, Raveendra et al. [8] synthesized nano $ZnTiO_3$ ceramic for the removal of azo dyes from aqueous solutions. Iron oxide nanospheres were synthesized by Khosravi et al. and

*Corresponding author.

used to remove anionic dyes from water [9]. Wu et al. used a hydrothermal procedure to prepare magnetic Fe_3O_4@C nanoparticles for dye adsorption [10].

Nanostructured titanium dioxide (TiO_2), which is a semiconductor material, is nontoxic, inexpensive, active in reactions, and chemically stable [11–14]. Therefore, it has many applications, including its use as an adsorbent [7,15,16]. TiO_2 has also been applied to remove anionic dye pollutants from wastewaters. The main issue in applying TiO_2 as an adsorbent is the problem of separation from an aqueous medium. Separation techniques, such as membrane filtration [17] are expensive. Yet commercial TiO_2 does not show a very high adsorption capacity for dye removal compared to activated carbons [6]. Doping the other materials to TiO_2 is an effective method to improve its adsorbent and photocatalytic character, also enhancing the separation efficiency.

The modification of TiO_2 with carbon creates a synergetic effect established by the adsorption capacity of activated carbon and the photoactivity of TiO_2 [11,18,19]. Carbon-modified TiO_2 has been used to adsorb azo dyes, such as reactive red 198 and direct green 99, [1] or reactive black 5 diazo dye [20]. These studies show that the combination of activated carbons and TiO_2 nanoparticles can produce a proper adsorbent which has both high adsorption capacity and excellent photocatalytic activity.

In the present study, carbon-modified TiO_2 (C–TiO_2) was prepared by ethanol carbonization and used for the removal of methyl orange (MO) dye pollutant from aqueous solution. The characterization of the prepared adsorbents was carried out by SEM images, N_2 adsorption/desorption isotherm, and XRD patterns. UV–vis spectroscopy was used to follow the adsorption process. The adsorption equilibrium, adsorption kinetics, and the effect of pH on dye removal efficiency were investigated. The effect of carbonization temperature on the zeta potential (ZP) and removal efficiency of MO by the prepared adsorbents was also studied. The ability to recover an alternative adsorbent is important from both an economic and a practical perspective. Thus, desorption studies were also performed.

2. Experimental

2.1. Materials

MO sodium salt dye was supplied by J.T. Baker and used without further purification. TiO_2 (nanopowder avg size = 25 nm with a chemical purity of ≥99.5) was purchased from Sigma–Aldrich and used as a precursor for the modification of TiO_2 (C–TiO_2).

2.2. Instruments

MO concentration was analyzed by UV–vis spectroscopy using a Jasco V-670 spectrophotometer (Jasco, Japan). The X-ray diffraction (XRD) patterns of modified TiO_2 were obtained with a PANalytical ŹPert PRO alpha 1 diffractometer. Cu Kα1 radiation (1.5406 Å; 45 kV, 30 mA) was used, generated by primary beam Johansson monochromator. The Hitachi S-4800 (Hitachi, Japan) Ultra-High Resolution Scanning Electron Microscope (SEM) was used to analyze the morphology and size of the adsorbents.

N_2 adsorption–desorption isotherms were obtained with an ASAP2010 (Micromeritics). The samples were outgassed at 100˚C for 12 h, before nitrogen adsorption. The pore volume distributions as a function of pore size was calculated based on the Dubinin–Radushkevich equation using adsorption branches of the measured isotherm.

FTIR type Vertex 70 by Bruker Optics (Germany) was used to identify the surface functional groups of the prepared adsorbents. The FTIR spectra were recorded at 4 cm^{-1} resolution from 400 to 4,000 cm^{-1} and 100 scans per sample. The surface charge and point of zero charge of the modified and unmodified TiO_2 were determined by isoelectric point titration as a function of pH using a Zetasizer Nano ZS (ZEN3500, Malvern). The determination of carbon was obtained using an Organic Elemental Analyzer Flash 2000 (Thermo Scientific, Germany).

2.3. Preparation of carbon-modified TiO_2

The carbon-modified TiO_2 was prepared using the method described by Janus et al. [21]. The installation setup used for adsorption preparation is schematically shown in Fig. 1.

Briefly, 1 g of TiO_2 in a porcelain boat was modified with carbon by heating up to the specified temperature with a pipe furnace under ethanol vapor for 40 min and maintaining that temperature for 1 h. The ethanol vapor was prepared by bubbling pure argon through ethanol at room temperature.

Commercial TiO_2 consists of a mixture of anatase/rutile phases [22]. Previously, we have shown that up to 600˚C the phase ratio of anatase to rutile remained nearly constant and phase transition was not observed [6]. Thus, to investigate only the influence of carbonization temperature on the removal efficiency of C–TiO_2 adsorbents, these were synthesized at temperatures of 200, 300, and 400˚C. The C–TiO_2 samples were identified as C–TiO_2-200, C–TiO_2-300, and C–TiO_2-400, based on their carbonization temperatures.

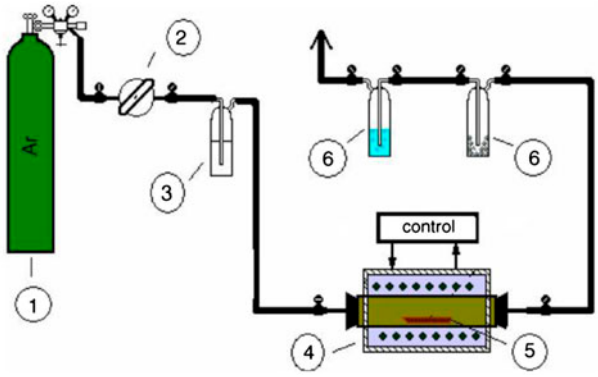

Fig. 1. Schematic presentation of installation setup for the synthesis of C–TiO_2 [21].
Notes: (1) Gas cylinder with argon, (2) controller, (3) Dreschel bottle with ethanol, (4) pipe furnace, (5) combustion boat with powder sample, and (6) scrubber.

2.4. Batch adsorption experiments

2.4.1. Adsorption kinetics and equilibrium

In order to evaluate the adsorption characterization of the synthesized adsorbents and to determine their adsorption capacity, adsorption kinetic and equilibrium studies were performed.

For the kinetic adsorption study 10 mL of a solution of 10 mg/L MO with 0.02 g of each C–TiO_2 adsorbents was placed in a shaker (200 rpm and 25°C) and the residual MO concentration at the proper time intervals, C_t, was determined at 473 nm. The amount of adsorbed MO per unit mass of the adsorbents at time t, q_t, was calculated by Eq. (1):

$$q_t = \frac{C_0 - C_t}{m} \times V \tag{1}$$

where C_0 (mg/L) is the initial concentration of the dye, V (L) is the solution volume, and m (g) is the mass of the adsorbent.

For the equilibrium experiments, a series of solutions with different initial concentrations (4–18 mg/L) were prepared, then 10 mL of each solution with 0.02 g of the desired adsorbent was placed in a shaker (200 rpm and 25°C) for 24 h. The equilibrium concentration of MO and C_e was measured at 473 nm, and the amount of adsorbed dye per unit mass of the adsorbent at equilibrium, q_e, was calculated using Eq. (2):

$$q_t = \frac{C_0 - C_e}{m} \times V \tag{2}$$

2.5. Effect of pH

To investigate the adsorption efficiency of C–TiO_2 adsorbents at different pH, a series of MO solutions (6 mg/L) with different initial pH (2–10) were prepared, and 10 mL of each solution with 0.02 g of the desired adsorbent was shaken overnight. The removal percentage of MO was calculated by Eq. (3):

$$\%\,\mathrm{Re} = \frac{A_0 - A}{A_0} \times 100 \tag{3}$$

where A_0 and A are the initial and equilibrium absorbance of MO at 473 nm, respectively.

2.6. Zeta potential

ZP is the electrical potential in the double layer at the interface between a particle, which moves in an electrical field and the surrounding liquid. Measuring ZP is also a method of characterizing the particle surface in the processes running on this surface. In this work, triton was used as a dispersing agent to predisperse the adsorbents in deionized water. To determine the ZP, 0.053 g of adsorbent and 0.25 mL of triton were added to 25 mL of deionized water and stirred for 10 min. This was then filled up to 50 mL with deionized water and subsequently mixed for 10 min. Next, the solution with a dilution ratio of 1:50 was stirred for 20 min.

2.7. Desorption experiments

Five adsorption/desorption cycles were performed to evaluate C–TiO_2 adsorbent efficiency after recovery.

Firstly, 0.2 g of the desired adsorbent was loaded onto 50 mL of the MO solution with an initial concentration of 200 (mg/L), overnight. Then the adsorbent was separated and washed several times to remove unadsorbed MO traces. The adsorbent was dried in an oven at 80°C overnight. The dried adsorbent was then washed with NaOH solution (1 M) several times until the elute pH became neutral. The adsorbent was washed with distilled water again and dried in an oven (80°C, overnight). In order to evaluate the removal efficiency of the recovered adsorbent, the above procedure was repeated another four times. Since an amount of adsorbent is lost during elution, the ratio between the mass of the adsorbent and the volume of the MO solution was kept at 4 ($m_{ad}/V_{sol} = 4$). After each cycle, the removal percentage of MO by recovered C–TiO_2 adsorbents was calculated by Eq. (4):

$$\%\,\mathrm{Re} = \frac{(A_0 - A)}{A_0} \times 100 \quad (4)$$

where A_0 and A are the initial and equilibrium absorbance of MO at 473 nm in each cycle.

3. Results and discussion

3.1. Characterization of C–TiO_2 adsorbents

The surface structures of the C–TiO_2 adsorbents were studied by SEM images. It can be seen from Fig. 2 that, all the C–TiO_2 samples consist of nanometer-size particles, like the TiO_2 precursor (Fig. 2(a)). The particle sizes of the TiO_2, C–TiO_2-200, and C–TiO_2-300 samples are about 30 and 50 nm (most particles are sized > 50 nm), respectively, and C–TiO_2-400 adsorbent (Fig. 2(d)) consists of particles with various sizes (20–60 nm). Thus, increasing the carbonization temperature to 300˚C increased the particle size (Fig. 2(b–d)).

Fig. 3 shows the nitrogen adsorption/desorption isotherm of the obtained adsorbents. The type IV isotherm and textural properties of C–TiO_2 samples listed in Table 1 reveal that the obtained adsorbents have a mesoporous structure. Table 1 also shows that the total surface area was slightly increased by increasing the carbonization temperature. These data correspond to the SEM images.

The effect of carbonization temperature on the crystalline phase of C–TiO_2 samples was studied by XRD technique. Fig. 4 shows the XRD patterns of the prepared adsorbents and TiO_2 precursor. It can be concluded that when TiO_2 nanoparticles were heated up to 400˚C, no phase transition occurred, which is in agreement with our previous work [6].

The FTIR spectra of the modified and unmodified TiO_2 are presented in Fig. 5. It can be observed that with increasing temperature, a new peak appeared in the range of 2,850–3,000 cm^{-1} assigned to the methyl group. This indicates not only the presence of ethanol in carbonization, but also that temperature can be related to the increased amount of carbon on modified TiO_2 nanoparticles. This finding is in agreement with the obtained elemental analysis results: The highest carbon content was found in C–TiO_2-400 (6.3%), compared to 0.12 and 4.53% for C–TiO_2-200 and C–TiO_2-300, respectively. This marked increase in carbon content also corresponds to the introduction of a methyl group on the TiO_2 surface.

3.2. Kinetic and equilibrium studies

A high adsorption rate is very desirable in water purification applications.

Fig. 6 shows the time dependency of the adsorption of MO by C–TiO_2 adsorbents. In each case, the dye removal was achieved within less than 60 min.

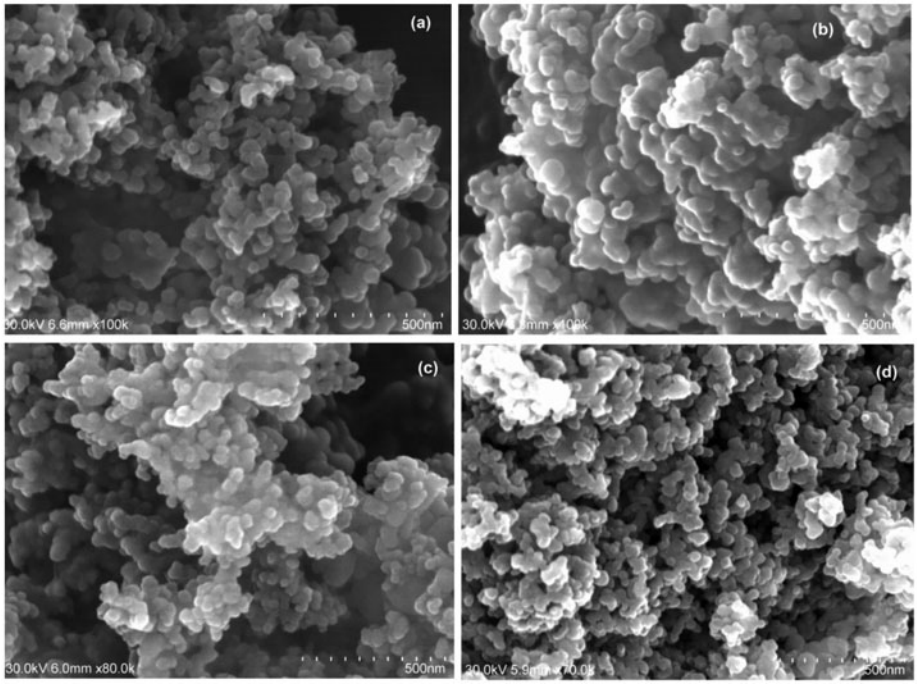

Fig. 2. SEM of (a) unmodified TiO_2, (b) C–TiO_2-200, (c) C–TiO_2-300, and (d) C–TiO_2-400. The scale bar represents 500 nm.

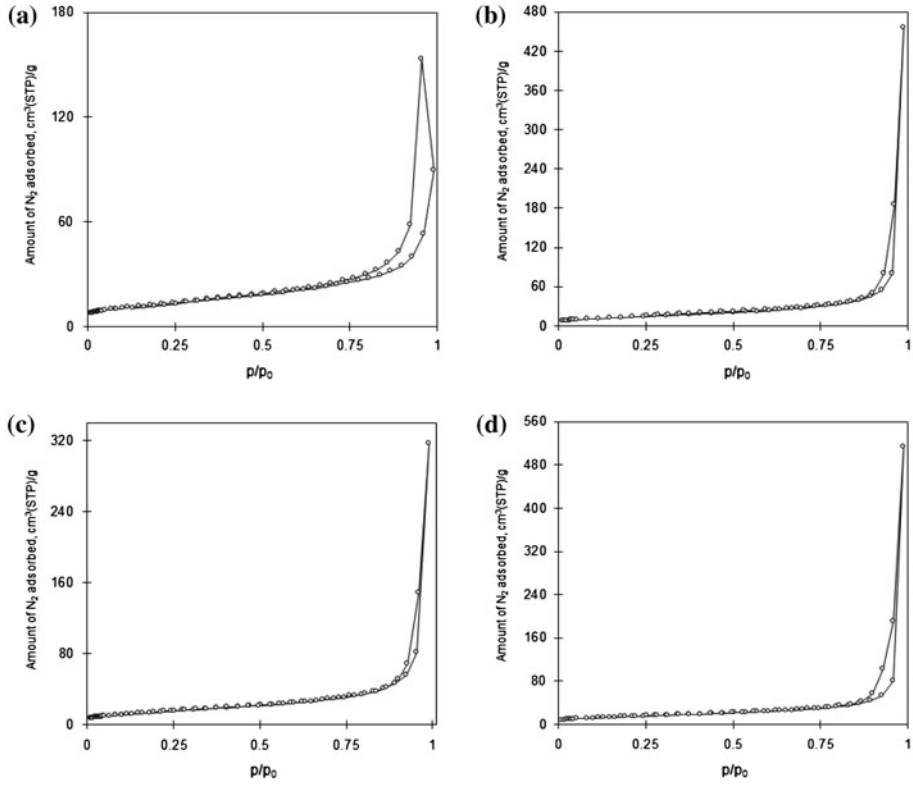

Fig. 3. Nitrogen adsorption/desorption isotherm of (a) TiO_2, (b) C–TiO_2-200, (c) C–TiO_2-300, and (d) C–TiO_2-400.

Table 1
Textual properties of TiO_2 and C–TiO_2 adsorbents

Adsorbent	S_{BET} (m^2/g)	$V_{total\ 0.95}$ (cm^3/g)	$V_{mikro\ DR}$ (cm^3/g)	V_{mezo} (cm^3/g)
TiO_2	44	0.0163	0.016	0.003
C–TiO_2-200	51	0.710	0.020	0.690
C–TiO_2-300	52	0.49	0.020	0.47
C–TiO_2-400	53	0.790	0.020	0.770

The adsorption rate increased further with rising carbonization temperature. This result corresponds to the results of the nitrogen adsorption/desorption isotherm and SEM images. Indeed, the increase in adsorbent surface area with rising carbonization temperature leads to the increase in adsorption rate.

The kinetic data were analyzed with pseudo-first-order (PFO) and pseudo-second-order rate equations [6]. The integrated form of the PFO model can be expressed as:

$$q_t = q_e(1 - \exp(-k_1 t)) \tag{5}$$

where q_t and q_e are the amounts of the dye adsorbed at time t and at equilibrium e, respectively, and k_1 is the PFO rate coefficient.

The following equation shows the pseudo-second-order (PSO) model [6]:

$$q_t = \frac{k_2 q_e^2 t}{1 + k_2 q_e t} \tag{6}$$

where k_2 is the pseudo-second-order rate coefficient.

According to the obtained correlation coefficients, the experimental kinetic data were best fitted to the pseudo-second-order equation for the adsorption of MO onto the C–TiO_2 adsorbents. The fitting results are listed in Table 2. The solid lines in Fig. 6 show the predicted values of q_t based on the PSO model as a function of time.

Fig. 7 shows the equilibrium data of MO adsorption onto the prepared adsorbents. These data show

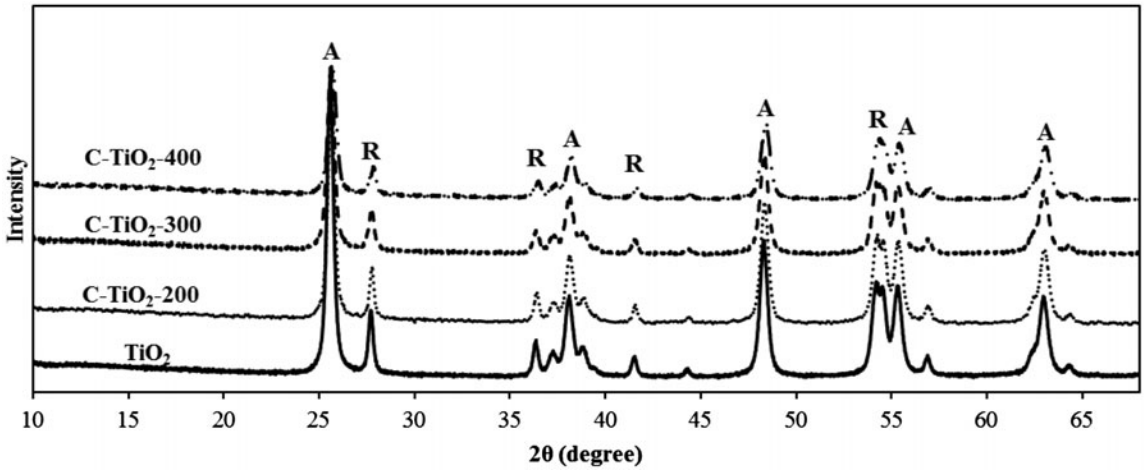

Fig. 4. XRD patterns of the prepared adsorbents and TiO_2 precursor.

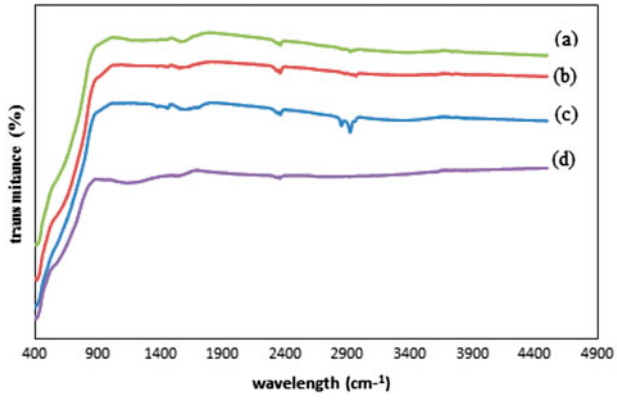

Fig. 5. FTIR spectra of modified and unmodified TiO_2, (a) C–TiO_2-200, (b) C–TiO_2-300, (c) C–TiO_2-400, and (d) TiO_2.

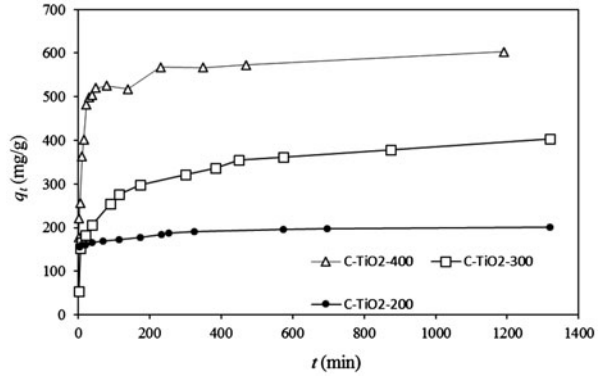

Fig. 6. Time dependency of the adsorption of MO by C–TiO_2 adsorbents. Solid and dashed lines represent the predicted q_t values by PSO model.

that while carbonization at 300 and 400˚C increases the adsorption capacity of C–TiO_2-300 and C–TiO_2-400 in comparison to unmodified TiO_2, carbonization at 200˚C has no significant effect on C–TiO_2-200 adsorption capacity. Thus, it can be concluded that, although, carbon modification of TiO_2 at 200˚C increases its surface area (Table 1), which could also improve the adsorption efficiency, a large surface area does not always indicate efficient adsorption. The surface charge of adsorbents also plays a significant role in the adsorption process, and seems more important for high adsorption capacity, as discussed below.

Langmuir, Freundlich, Langmuir–Freundlich, and Temkin isotherms were used to analyze the experimental equilibrium data, and to obtain the maximum adsorption capacity of synthesized C-TiO_2 adsorbents for MO dye removal.

The Langmuir isotherm can be expressed as follows [23]:

$$q_e = \frac{q_m K_L C_e}{1 + K_L C_e} \tag{7}$$

where q_m (mg/g) and K_L (L/mg) are the maximum adsorption capacity and Langmuir constant, respectively.

The following equation shows the Freundlich isotherm which described the multisite adsorption [24]:

$$q_e = K_F C_e^{1/n} \tag{8}$$

where K_F (mg/g) $(L/mg)^{1/n}$ is the Freundlich constant, and the parameter n describes the system heterogeneity.

Table 2
Obtained constants of PFO and PSO rate equations for the adsorption of MO onto C–TiO_2 adsorbents

	PFO			PSO		
Adsorbent	q_e (mg/g_{ads})	k_1 (1/min)	r^2	q_e (mg/g_{ads})	k_2 (g_{ads}/mg min)	r^2
C–TiO_2-200	201.3	0.0050	0.9642	200.00	0.00038	0.9996
C–TiO_2-300	403.9	0.0044	0.8962	400.00	0.00006	0.9955
C–TiO_2-400	520.1	0.1506	0.8644	588.235	0.00030	0.9956

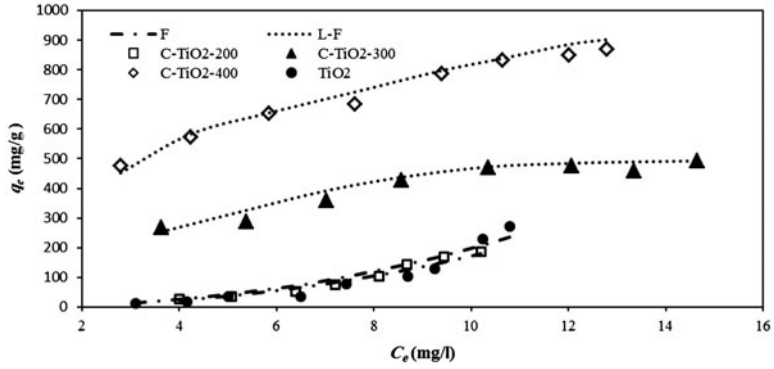

Fig. 7. Adsorption isotherm of MO onto TiO_2 and C–TiO_2 adsorbents at 25°C.

The Langmuir–Freundlich (Sips) isotherm, which is a combination of the Langmuir and Freundlich isotherms, can be expressed as follows [25]:

$$q_e = \frac{q_m K_s C_e^{1/n}}{1 + K_s C_e^{1/n}} \quad (9)$$

where K_s $(1/mg)^{1/n}$ is the adsorption constant.

The Temkin isotherm, [26] which is a two-parameter adsorption isotherm, can be expressed as below:

$$q_e = \alpha \ln(\beta C_e) \quad (10)$$

where α and β are the isotherm constants.

The results of fitting to the adsorption isotherm models are listed in Table 3. According to the obtained correlation coefficients, the experimental equilibrium data for the adsorption of MO onto TiO_2 and C–TiO_2-200 were fitted to the Freundlich isotherm and those for adsorption onto C–TiO_2-300 and C–TiO_2-400 were best fitted to the Langmuir–Freundlich isotherm. The predicted values of q_e based on the Langmuir–Freundlich equation are presented in Fig. 7 as solid lines.

3.3. Effect of pH and ZP

The pH of the solution is an effective function in dye removal efficiency, especially in the case of semiconductor adsorbents. Thus, the removal percentages of MO by C–TiO_2 adsorbents were investigated at different pH.

Fig. 8(a–c) show the removal percentage of MO by carbon-modified TiO_2 adsorbents at different pH. The maximum removal efficiency was observed at pH 6 and 4 for C–TiO_2-200 and C–TiO_2-300, respectively. In the case of C–TiO_2-400, the maximum removal percentage was achieved in an acidic medium up to pH 4, and then decreased slightly. For C–TiO_2-200, C–TiO_2-300, and C–TiO_2-400, the point of zero charge (pH_{PZC}) was found to be at pH 6.53, 5.19, and 4.48, respectively, while the pH_{PZC} for unmodified TiO_2 was around 6.13 (data not shown). A change in pH_{PZC} after modification was caused by the presence of methyl groups on the surface of the modified TiO_2.

The adsorbent surface has a negative charge at solution pH higher than pH_{PZC}, while the surface charge is positive at pH lower than pH_{PZC} [27].

Fig. 9 shows the chemical structure of MO in acidic and basic media. In the case of C–TiO_2-200 and C–TiO_2-300, high removal efficiency was reached in an

Table 3
Obtained isotherm constants for adsorption of MO onto TiO_2 and C–TiO_2 adsorbents

Isotherm models		TiO_2	C–TiO_2-200	C–TiO_2-300	C–TiO_2-400
Langmuir	K_L (L/mg)	3.000	4.367	137.475	182.936
	q_m (mg/g)	0.0288	0.018	0.0007	0.0003
	r^2	0.8875	0.9584	0.7260	0.9668
Freundlich	K_F (L $mg^{(1-1/n)}$/g)	0.1822	1.059	141.982	321.436
	n	0.442	0.452	0.479	0.393
	r^2	0.9304	0.968	0.9307	0.9905
Langmuir–Freundlich	K_{L-F} (L/mg)	0.0624	0.057	0.0015	0.0018
	q_m (mg/g)	47.619	171.428	500.000	909.090
	n	0.90	0.90	0.25	0.25
	r^2	0.8714	0.9488	0.9982	0.9990
Tempkin	b	180.66	53.373	189.000	354.43
	r^2	0.6968	0.433	0.9271	0.8516

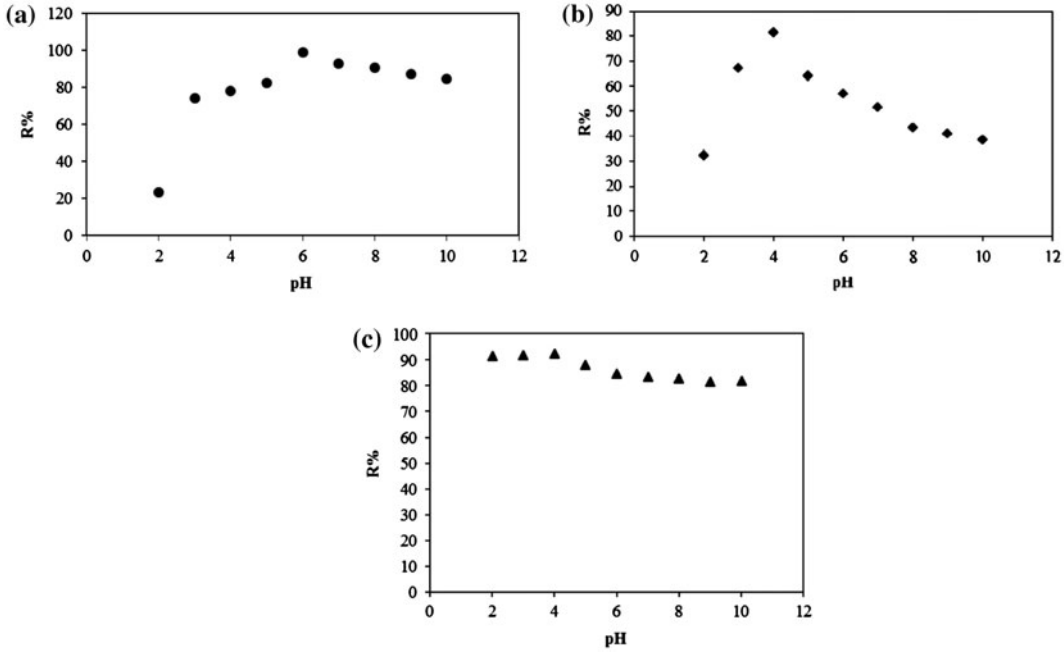

Fig. 8. Removal percentage of MO by (a) C–TiO_2-200 (b) C–TiO_2-300 and (c) C–TiO_2-400 at different pH.

acidic medium, while basic pH decreased the removal percentages. Thus, in acidic media (lower than pH_{pzc} of 6.53 and 5.19 for C–TiO_2-200 and C–TiO_2-300, respectively), the strong attractive interaction between the $-SO_3^-$ group of MO and positive surface of the mentioned adsorbents causes maximum removal efficiency. At basic pH, the repulsion interaction between the negative end of the MO molecules and negative surface of the C–TiO_2-200 and C–TiO_2-300 decreased the removal percentages.

As shown in Fig. 8(c), the removal percentage of MO by C–TiO_2-400 almost remains unchanged at acidic and basic pH. This suggests that MO molecules are not adsorbed through the ionic $-SO_3^-$ group [5]. It seems that MO adsorption is due to the interaction between the central nitrogen or benzene rings and the surface of C–TiO_2-400.

ZP was measured to illustrate the mechanism of the pH effect on MO removal efficiency by C–TiO_2 adsorbents. It was very difficult to make this type of modified TiO_2 nanoparticle disperse homogeneously into the aqueous solution, especially as dispersion takes a long time. Triton was therefore used to pre-disperse the adsorbents in deionized water. As can be seen from

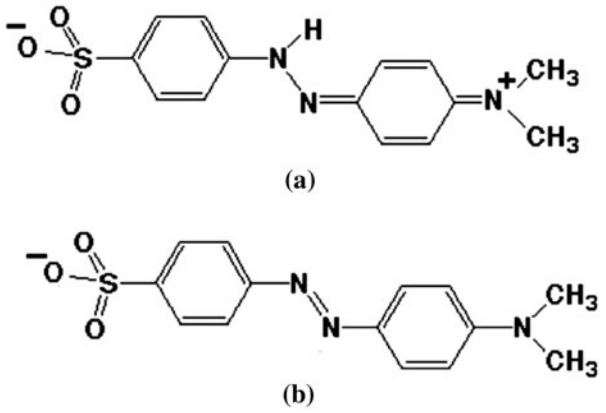

Fig. 9. MO structure at (a) acidic and (b) basic mediums.

Fig. 10, the TiO_2 surface has a highly negative ZP in suspension, leading to repulsion between particles. In contrast, the modified TiO_2 had a significantly lower ZP (the ZP of TiO_2, C–TiO_2-200, C–TiO_2-300, and C-TiO_2-400 are −32.2, −23.3, −15.2, and −10.8 mV, respectively). Thus, the decline in negative ZP not only leads to flocculation [1], but also causes better adsorption of MO onto modified TiO_2 than unmodified TiO_2. Furthermore, carbonization at 200˚C led to a slight decrease in the ZP of C–TiO_2-200 as compared to unmodified TiO_2, while adsorbents prepared at 300 and 400˚C demonstrated a large change in ZP. Thus, the adsorption capacity of unmodified TiO_2 and C–TiO_2-200 is almost the same (Fig. 7). The much lower ZP of C–TiO_2-300 and C–TiO_2-400 is due to their higher adsorption capacity. This may suggest that the electrostatic interaction between the dye-(C–TiO_2) complex and negatively charged surface of heat-treated TiO_2 becomes dominant. In addition, the interaction mechanism of dye molecules and the sample calcined at different temperatures are different; the interaction is stronger at high temperatures.

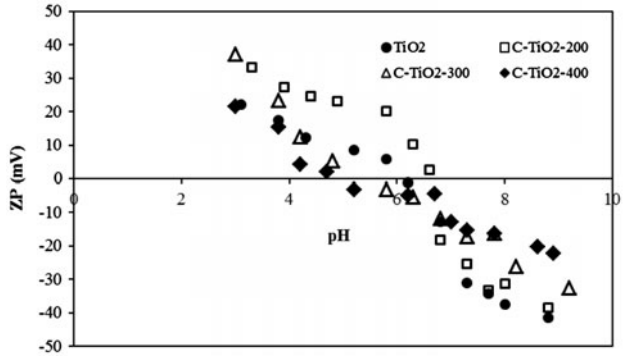

Fig. 10. ZPs of TiO_2 and C–TiO_2 adsorbents.

3.4. Desorption and regeneration studies

The results of the adsorption/desorption experiments are shown in Fig. 11. These results approve the electrostatic interaction between MO and C–TiO_2 adsorbents, since this interaction is limited by NaOH solution.

Although the removal efficiency decreased by 30, 24, and 19% after five cycles for C–TiO_2-200, C–TiO_2-300, and C–TiO_2-400, respectively, it remained above 50% for all C–TiO_2 adsorbents. Thus, all prepared adsorbents, especially C–TiO_2-400 (with its 19% efficiency decrease), could be reused at least five times, which is both highly economical and practical.

3.5. Adsorption mechanism

The Weber–Morris intraparticle diffusion model was applied to identify the adsorption mechanism of MO adsorption onto the modified TiO_2. This model, which includes terms to account for both intraparticle diffusion and boundary layer diffusion, is expressed as follows:

$$q_t = K_{dif} t^{0.5} + C_i \quad (11)$$

where K_{dif} (mg/g $min^{-0.5}$) is the rate constant of intraparticle diffusion and C_i (mg/g) stands for thickness of the boundary layer.

The plot of q_t vs. $t^{0.5}$ for MO adsorption on C–TiO_2-200, C–TiO_2-300, and C–TiO_2-400 are illustrated in Fig. 12. It can be seen from Fig. 12(a) that q_t was plotted against $t^{0.5}$ in a straight line with an intercept (C_i). This indicates that the intraparticle diffusion was important, but not the only rate-determining step in the adsorption process. Moreover, the obtained intercept value (C_i = 1.579 mg/g) is positive, indicating rapid adsorption in a short period of time. Furthermore, the

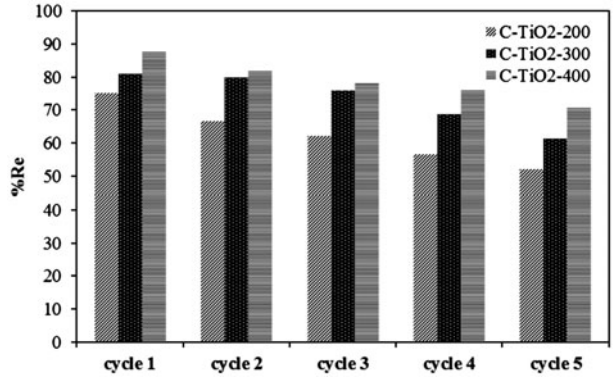

Fig. 11. Regeneration studies of C–TiO_2 adsorbent.

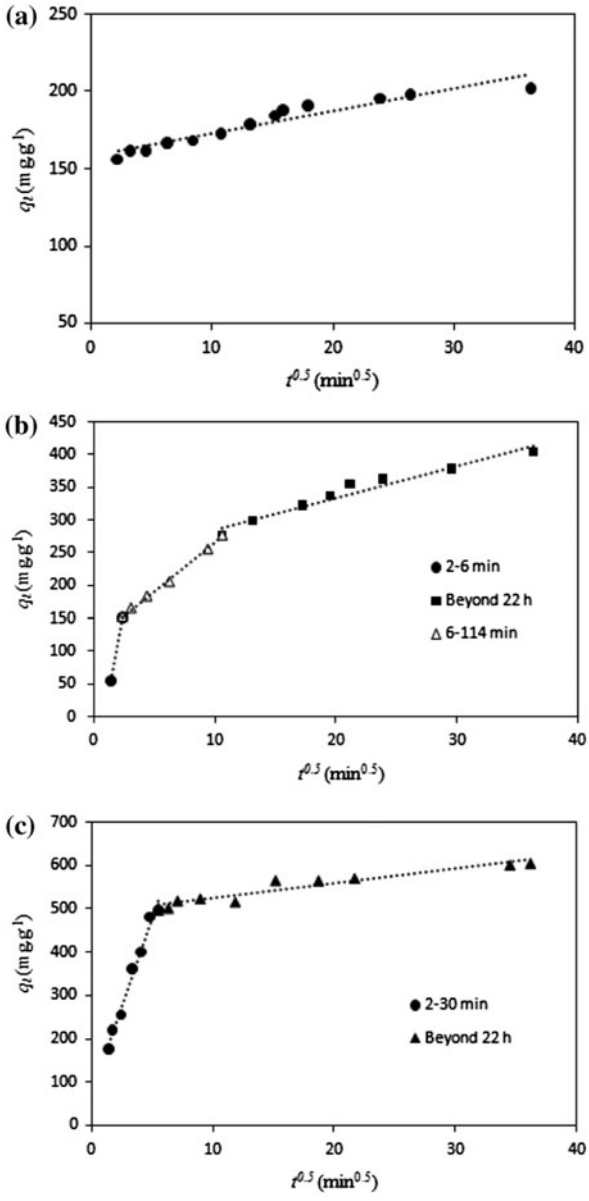

Fig. 12. The intraparticle diffusion plot for adsorption of MO onto (a) C–TiO_2-200, (b) C–TiO_2-300 and (c) C–TiO_2-400.

rate constant (K_{dif} = 0.145 mg/g min$^{0.5}$) indicates a rapid diffusion process. Fig. 12(b) and (c) shows the intraparticle diffusion plots for MO adsorption onto C–TiO_2-300 and C–TiO_2-400, which reveal the same general features as the multi-linear q_t vs. $t^{0.5}$ plot. The whole adsorption process for C–TiO_2-400 and C–TiO_2-300 consist of two and three steps, respectively. In C–TiO_2-300, the initial sharply sloped portion of 2–6 min may occur due to the small particle size noted above, indicating external surface adsorption. The second step is the gradual adsorption stage from 6 to 114 min, during which intraparticle diffusion may be the rate-limiting step. The third and final equilibrium stage beyond 22 h corresponds to the slowing down of intraparticle diffusion due to low solute concentrations in the solution. When adsorption has reached saturation on the exterior surface, the MO ions may have entered the pore surface, which is hydrated in liquid phase. In C–TiO_2-400 (Fig. 12(c)) an initial curved portion representing increased sorption is followed by a linear portion as equilibrium is attained. The primary linear portion at 2–30 min may be attributed to the external surface, and the second curved portion (beyond 22 h) may be ascribed to the pore diffusion or intraparticle diffusion. Two distinct linear regions of differing slopes are visible on the graph, indicating that intraparticle diffusion is involved in the adsorption process, but is not the only rate-limiting mechanism. Other mechanisms may also simultaneously control the rate of MO adsorption onto C–TiO_2-400; further investigation is required in order to describe these.

4. Conclusions

Carbon-modified TiO_2 adsorbents were prepared at different carbonization temperatures (200–400˚C), and used for the adsorptive removal of MO dye pollutant from aqueous solution. Our results show that MO dye pollutant was rapidly removed by all C–TiO_2 adsorbents; the adsorption process took less than 1 h. It was revealed that the MO adsorption capacity of TiO_2 increases by carbon modification. Changing the carbonization temperature had no significant effect on the surface area of TiO_2, but did enhance maximum adsorption capacity, which might be due to the increase in adsorbent ZP. The Freundlich adsorption model was found to fit well for TiO_2 and C–TiO_2-200, while carbon-modified TiO_2 fitted the Langmuir–Freundlich model at higher temperatures. All the prepared adsorbents could be regenerated at least five times and used as economical adsorbents in purification applications.

References

[1] M. Janus, E. Kusiak, J. Choina, J. Ziebro, A.W. Morawski, Enhanced adsorption of two azo dyes produced by carbon modification of TiO_2, Desalination 249 (2009) 359–363.
[2] J. Chen, L. Zhu, Catalytic degradation of Orange II by UV-Fenton with hydroxyl-Fe-pillared bentonite in water, Chemosphere 65 (2006) 1249–1255.
[3] E. Guibal, J. Roussy, Coagulation and flocculation of dye-containing solutions using a biopolymer (Chitosan), React. Funct. Polym. 67 (2007) 33–42.

[4] I. Kabdasli, M. Gürel, O. Tünay, Characterization and treatment of textile printing wastewaters, Environ. Technol. 21 (2000) 1147–1155.
[5] B. Yahyaei, S. Azizian, Rapid adsorption of anionic dyes by ordered nanoporous alumina, Chem. Eng. J. 209 (2012) 589–596.
[6] S. Jafari, S. Azizian, B. Jaleh, Adsorption kinetics of methyl violet onto TiO_2 nanoparticles with different phases, Colloids Surf., A: Physicochem. Eng. Aspects 384 (2011) 618–623.
[7] B. Tanhaei, A. Ayati, M. Lahtinen, M. Sillanpää, Preparation and characterization of a novel chitosan/Al_2O_3/magnetite nanoparticles composite adsorbent for kinetic, thermodynamic and isotherm studies of Methyl Orange adsorption, Chem. Eng. J. 259 (2015) 1–10.
[8] R.S. Raveendra, P.A. Prashanth, R. Hari Krishna, N.P. Bhagya, B.M. Nagabhushana, H. Raja Naika, K. Lingaraju, H. Nagabhushana, B. Daruka Prasad, Synthesis, structural characterization of nano $ZnTiO_3$ ceramic: An effective azo dye adsorbent and antibacterial agent, J. Asian Ceram. Soc. 2 (2014) 357–365, doi: 10.1016/j.jascer.2014.07.008.
[9] M. Khosravi, S. Azizian, Adsorption of anionic dyes from aqueous solution by iron oxide nanospheres, J. Ind. Eng. Chem. 20 (2014) 2561–2567.
[10] R. Wu, J.-H. Liu, L. Zhao, X. Zhang, J. Xie, B. Yu, X. Ma, S.-T. Yang, H. Wang, Y. Liu, Hydrothermal preparation of magnetic Fe_3O_4@C nanoparticles for dye adsorption, J. Environ. Chem. Eng. 2 (2014) 907–913.
[11] K. Bubacz, B. Tryba, A.W. Morawski, The role of adsorption in decomposition of dyes on TiO_2 and N-modified TiO_2 photocatalysts under UV and visible light irradiations, Mater. Res. Bull. 47 (2012) 3697–3703.
[12] A. Di Paola, G. Cufalo, M. Addamo, M. Bellardita, R. Campostrini, M. Ischia, R. Ceccato, L. Palmisano, Photocatalytic activity of nanocrystalline TiO_2 (brookite, rutile and brookite-based) powders prepared by thermohydrolysis of $TiCl_4$ in aqueous chloride solutions, Colloids Surf., A: Physicochem. Eng. Aspects 317 (2008) 366–376.
[13] B. Chládková, E. Evgenidou, L. Kvítek, A. Panáček, R. Zbořil, P. Kovář, D. Lambropoulou, Adsorption and photocatalysis of nanocrystalline TiO_2 particles for Reactive Red 195 removal: effect of humic acids, anions and scavengers, Environ. Sci. Pollut. Res. (2015) 1–11, doi: 10.1007/s11356-015-4806-y.
[14] S. Sabar, M.A. Nawi, W.S.W. Ngah, Photocatalytic removal of Reactive Red 4 dye by immobilised layer-by-layer TiO_2/cross-linked chitosan derivatives system, Desalin. Water Treat. 1–7, doi: 10.1080/19443994.2015.1004113(2015).
[15] S. Helali, E. Puzenat, N. Perol, M.-J. Safi, C. Guillard, Methylamine and dimethylamine photocatalytic degradation—Adsorption isotherms and kinetics, Appl. Catal. A: Gen. 402 (2011) 201–207.
[16] A.A. Vega, G.E. Imoberdorf, M. Mohseni, Photocatalytic degradation of 2,4-dichlorophenoxyacetic acid in a fluidized bed photoreactor with composite template-free TiO_2 photocatalyst, Appl. Catal. A: Gen. 405 (2011) 120–128.
[17] H. Han, R. Bai, Effect of thickness of photocatalyst film immobilized on a buoyant substrate on the degradation of methyl orange dye in aqueous solutions under different light irradiations, Ind. Eng. Chem. Res. 50 (2011) 11922–11929.
[18] J. Matos, J. Laine, J.M. Herrmann, Association of activated carbons of different origins with titania in the photocatalytic purification of water, Carbon 37 (1999) 1870–1872.
[19] J. Matos, J. Laine, J.M. Herrmann, Effect of the type of activated carbons on the photocatalytic degradation of aqueous organic pollutants by UV-irradiated Titania, J. Catal. 200 (2001) 10–20.
[20] M. Janus, E. Kusiak, A. Morawski, Carbon modified TiO_2 photocatalyst with enhanced adsorptivity for dyes from water, Catal. Lett. 131 (2009) 506–511.
[21] M. Janus, M. Inagaki, B. Tryba, M. Toyoda, A. Morawski, Carbon-modified TiO_2 photocatalyst by ethanol carbonisation, Appl. Catal. B 63 (2006) 272–276.
[22] M.-H. Baek, J.-W. Yoon, J.-S. Hong, J.-K. Suh, Application of TiO_2-containing mesoporous spherical activated carbon in a fluidized bed photoreactor—Adsorption and photocatalytic activity, Appl. Catal. A: Gen. 450 (2013) 222–229.
[23] I. Langmuir, The adsorption of gases on plane surfaces of glass, mica and platinum, J. Am. Chem. Soc. 40 (1918) 1361–1403.
[24] H. Freundlich, Over the adsorption in solution, J. Phys. Chem. 57 (1906) 385–470.
[25] R. Sips, On the structure of a catalyst surface, J. Chem. Phys. 16 (1948) 490–495.
[26] B. Saha, C. Orvig, Biosorbents for hexavalent chromium elimination from industrial and municipal effluents, Coord. Chem. Rev. 254 (2010) 2959–2972.
[27] N. Fiol, I. Villaescusa, Determination of sorbent point zero charge: usefulness in sorption studies, Environ. Chem. Lett. 7 (2009) 79–84.